Journal of Ceramic Processing Research. Vol. 7, No. 4, pp. 321~326 (2006)

J O U R N A L O F
Ceramic Processing Research

Stable antimony-doped tin oxide nano-sols and their films produced by a sol-coating method

Seong Je Jeon, Jai Joon Lee, Jun Tae Kim and Sang Man Koo*
Department of Chemical Engineering, Ceramic Processing Research Center, College of Engineering, Hanyang University, Seoul 133-791, Korea

The preparation of ethanol-based antimony-doped tin oxide (ATO) nano-sols and their films are described. Aggregates of antimony-doped tin oxide (ATO) nanoparticles were synthesized by a hydrothermal method in an autoclave. After peptization with tetramethylammonium hydroxide and solvent-exchange to ethanol, highly stable ethanol-based ATO nano-sols with solid contents up to 20 wt% were prepared. Transparent ATO films were formed on polyethylene terephthalate (PET) films using the ATO nano-sol by a spin coating method. The effects of antimony content and solid content on packing density and the resistivity of the ATO films were studied.

Key words: Antimony-doped tin oxide, peptization, resistivity, transparency.

Introduction

Transparent conducting oxides (TCOs) have been widely studied for energy storage devices, transparent electrodes, catalyst and gas sensors, and heat reflecting mirrors [1-9] because they exhibit good transparency and electrical conductivity. Indium tin oxide (ITO) has been widely used among the various TCOs. However, disadvantages in its use include the high expense of indium and the difficulty of etching it by wet chemical methods during the patterning process. For these reasons, much research has focused on SnO_2-based TCOs as alternatives to ITO. For example, there have been many reports about the conductivity and physical properties of SnO_2 thin films containing various impurities such as antimony (Sb), fluorine (F), niobium (Nb), cadmium (Cd), molybdenum (Mo) or zinc (Zn) [10-17].

TCO films can be fabricated by various methods such as spray pyrolysis [18, 19], chemical vapor deposition [20, 21], sputtering [22], electron beam evaporation [23], thermal oxidation [24], and sol-gel coating [25-34]. In particular, sol-gel coating techniques are attractive due to their ability to produce homogeneous and transparent TCO films with various dopants for large-scale production [35]. However, sol-gel coating techniques tend to produce films with substantial porosity and, therefore, lower conductivity than other films produced by vapor phase methods such as sputtering. Recently, sol-coating methods using a stable TCO particulate sol has been attempted in order to improve these properties.

In this study, we synthesized an antimony-doped tin oxide (ATO) particulate sol with a high concentration and prepared its homogeneous films by a sol-coating method using a spin coater. We also studied the electrical and optical properties of the ATO films as a function of the crystallite size, solid content and antimony content of the ATO sol.

*Corresponding author:
Tel : +82-2-2220-0527
Fax: +82-2-2281-4800
E-mail: sangman@hanyang.ac.kr

Experimental Procedure

Materials

Tin powder (Sn, Aldrich, 99.5%), antimony (III) oxide (Sb_2O_3, Aldrich, 99%), ammonium hydroxide (NH_4OH, Acros, 28-30%), nitric acid (HNO_3, Samchun chemical, 60%), water-based tetramethylammonium hydroxide (TMAH, Aldrich, 1.0 M aqueous solution), anhydrous ethyl alcohol (EtOH, J.T. Baker, 99.9%), potassium hydroxide (KOH, Shinyo pure chemical, 85%) and sodium hydroxide (NaOH, Shinyo pure chemical, 93%) were used as received. Water was purified by distillation and deionization.

The Preparation of ATO Sols

One gram of Sn and the appropriate amount of Sb_2O_3 powder were dissolved in 300 ml of aqueous solution with 30 ml nitric acid. The amount of Sb_2O_3 was varied to produce [Sb]/[Sn] molar ratios from 2.5-20.0. The resulting solution was vigorously stirred at room temperature for 60 minutes. The yellow solution was poured into a 400 ml autoclave vessel and heated at 170 °C for 12 hours. The resulting blue-colored ATO suspension was removed from the autoclave, cooled down to room temperature and washed with water. The

resulting blue ATO cake was peptized in an aqueous solution of TMAH (pH of 12.0) at 60 °C for 4 hours to produce the aqueous particulate ATO sol.

In order to obtain an ethanol-based ATO coating sol, the resulting aqueous ATO sol was evaporated at 80 °C in a rotary evaporator under reduced pressure. The dried ATO powders could then be easily redispersed in ethanol with various solid contents.

Formation of ATO Films

ATO films were formed using 2 ml of the ethanol-based ATO coating sol by spin-coating on polyethylene terephthalates (PET) substrates with a radius of 2.5 mm and a thickness of 0.1 μm. The spin-coating was conducted in three stages: 5000 rev./minute for 45 seconds, 7000 rev./minute for 45 seconds, and 5000 rev./minute for 45 seconds. The coated ATO films were then dried at 80 °C for 6 hours in a vacuum oven.

Characterization of films

Fourier transform infrared spectroscopy analysis (FT-IR, Avatar 360 FT-IR spectrometer) was undertaken to confirm the residual organic moieties in the dried ATO particles. The phases and crystallite sizes of ATO particles were identified with an X-ray diffractometer (XRD, Rint-2000, Rigaku) using Cu-Kα_1 radiation at 40 kV and 100 mA. The size and morphology of the ATO particles were observed by high resolution-transmission electron microscopy (HR-TEM, JEM-3010, Jeol) at an accelerating voltage of 300 kV. The samples for HR-TEM were diluted in ethanol, loaded on carbon-coated grids and dried at room temperature. The surface of the ATO films was examined by field emission-scanning electron microscopy (FE-SEM, JSM-6700F, Jeol).

The electrical conductivity of the film was measured by a four-point probe (CMT-SR2000N, Jandel, U.K.) technique. The thickness of films was determined by means of a scanning probe microscope (SPM, SPA-400, Seiko Instruments Inc.) and a Tencor alpha step surface profiler. The transmittance of ATO coating sols and their films were measured in the wavelength range of 300-800 nm using a UV/Vis spectrophotometer (Optizen 2120 UV, Mecasys Co., Ltd.). A blank sample of an uncoated PET substrate was used as a reference in the measurement of optical transmittance and thickness. The binding energies of Sb $3d_{3/2}$ level in the ATO films were analyzed by X-ray photoelectron spectroscopy (XPS, ESCA 2000, VG Microtech Ltd.) to investigate the oxidation number of Sb. The XPS measurements were performed with a base pressure of 10^{-9} mbar using a Cameca Nano-scan 50 microprobe with Al Kα_1 non-chromatized x-ray source (350W) and hemispherical analyzer at a passed energy of 11 eV.

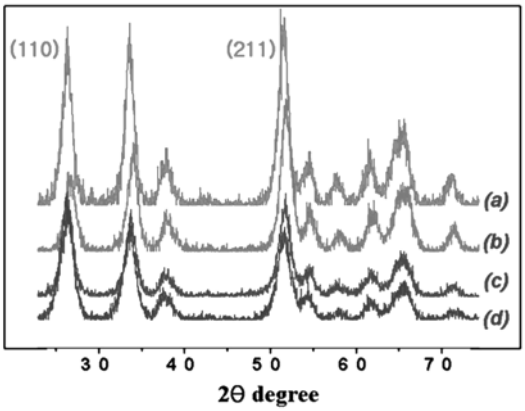

Fig. 1. XRD patterns of SnO_2 nanoparticles doped with Sb; (a) 0, (b) 5.0, (c) 10.0, and (d) 20.0 mol% Sb.

Results and Discussion

X-ray diffraction patterns (Fig. 1) for ATO nanoparticles doped with Sb (0-20 mol% Sn) indicate that the ATO particles have a cassiterite structure similar to that of the pure SnO_2. No peaks related with Sb such as Sb_2O_3 were observed even in the sample doped with 20 mol% of Sb (Fig. 1(d)). It was also observed that the XRD peaks of ATO nanoparticles became significantly broadened with increasing Sb doping content. The crystallite sizes of the ATO particles could be calculated from (211) peaks of the XRD patterns by use of the Scherrer equation and decreased from 4.8 nm for pure SnO_2 to 2.2 nm for 20 mol% of Sb-doped SnO_2 particles. Our results correspond with those of Pyke et al. [36] who also observed that the ATO crystallites became smaller with increasing antimony doping content. The inhibition of growth for ATO particles with increased Sb doping content is also seen in HR-TEM images where the average particle size of SnO_2 decreased with increasing Sb doping content (Fig. 2).

We used TMAH as the peptizing agent for preparing the stable aqueous ATO sol from the precipitates obtained via the autoclave reaction mentioned before. Although stable aqueous ATO sols could be obtained using other inorganic bases such as NaOH, KOH, and NH_4OH rather than TMAH, they could not be redispersed in alcohol solutions after evaporation. Therefore, TMAH was thought to remain on the surface of the evaporated ATO particles facilitating them to redisperse in alcohol solutions. Figure 3 shows FT-IR spectra of pure TMAH and the evaporated ATO particles prepared with TMAH. The broad band around 3478 cm^{-1} is assigned to the surface-adsorbed water, while the sharp peak at 3010 cm^{-1} originates from the O-H group of TMAH. Also, peaks corresponding to the aliphatic C-H bonds are detected between 2910-2980 cm^{-1}, 2930, 1470, and 1345 cm^{-1} in Fig. 3(a) and (b). Therefore,

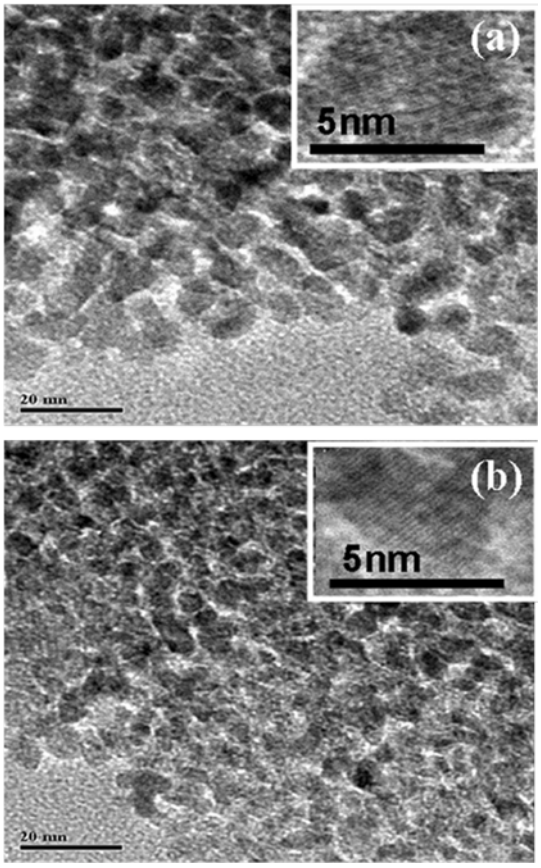

Fig. 2. HR-TEM images of SnO_2 nanoparticles doped with Sb; (a) 5.0 and (b) 10.0 mol% Sb. Insets are their enlarged images.

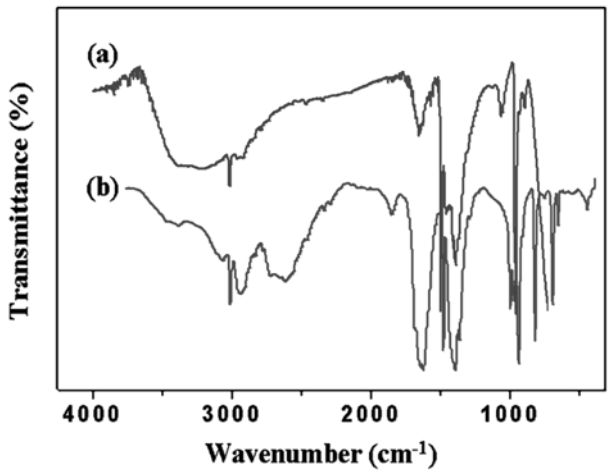

Fig. 3. FT-IR spectra of (a) 10.0 mol% Sb of Sb-doped SnO_2 nanoparticles peptized with TMAH after drying at 80 °C under reduced pressure and (b) pure TMAH dried at 100 °C.

the FT-IR analysis confirmed that TMAH remained in the evaporated ATO particles allowing them to redisperse in ethanol.

ATO films could be formed by a spin coating method with the stable ethanol-based ATO sol. The relationship between the thickness of the films and solid contents of the ATO sols was studied and is shown in Fig. 4. The

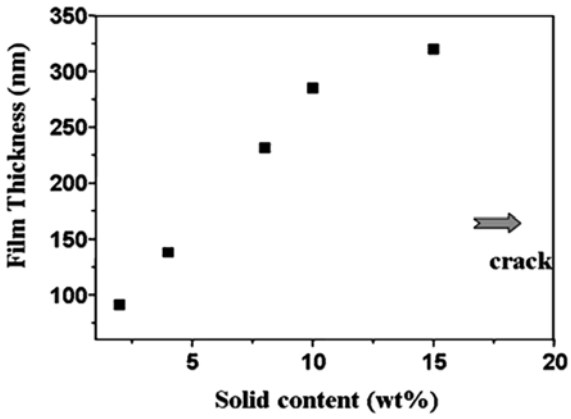

Fig. 4. The relationship between the solid content of the ATO sols (doped with 10 mol% Sb) and thicknesses of the resulting films.

film thickness increased from about 90 to 305 nm with the solid content from 2 to 15 wt% due to the increased viscosity of the sol [37]. Visible cracks were detected in the surface of the thick films when the films were prepared with the ATO sol content was above 20 wt%. It is believed that the additional stress introduced into the films exceeded a critical thickness causing crack formation. As a consequence, we could obtain crack-free ATO films with thicknesses of 90-305 nm using the ethanol-based ATO sols.

Figure 5 exhibits FE-SEM images of ATO films with various antimony contents produced by a spin coating method. The density of the ATO films increased and the particle size decreased as compared with that of pure SnO_2 films (Fig. 5(a)), which was also observed by XRD analysis in Fig. 1. However, the particle size increased at antimony contents above 10 mol% (Fig. 5(d)). This might be caused by some amorphous antimony compound forming at the surface of ATO particles. According to the XRD results (Fig. 1), ATO particles with an antimony content of 20 mol% had the smallest

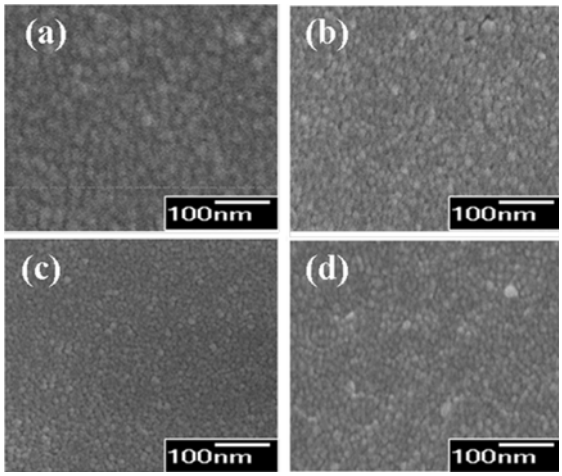

Fig. 5. SEM images of ATO film surfaces; (a) pure SnO_2 film, (b) doped with 5.0 mol% Sb, (c) doped with 10.0 mol% Sb, and (d) doped with 20.0 mol% Sb.

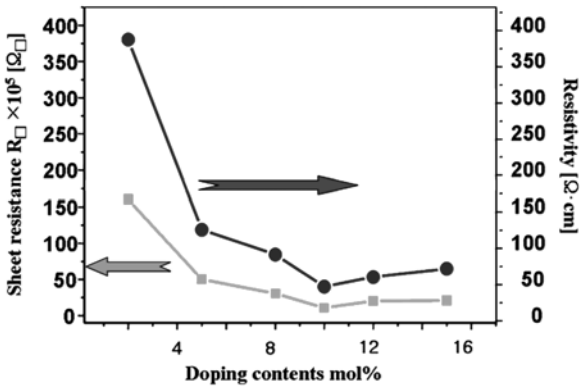

Fig. 6. Variations of sheet resistance and resistivity of ATO films with antimony content from 2 to 15 mol% at a fixed solid content of 8 wt%.

crystallite size and did not have any secondary phase except SnO_2. Therefore, the increased particle size in ATO samples with antimony contents above 10 mol% is not thought to originate from the grain growth of the ATO particles themselves.

The electrical resistivity was measured for the ATO films with various Sb doping contents as shown in Fig. 6. The resistivity value of the ATO film decreased with increasing antimony content of the sol and reached a minimum value of 40.1 Ω·cm for an antimony content of 10 mol%. However, the electrical resistivity increased significantly with further addition of Sb. This result agrees well with the FE-SEM results seen in Fig. 5. Shanthi et al. [38] have shown that nano-crystallite ATO films with higher crystallinity in the XRD patterns had lower resistivity. However, the ATO particles with the smallest particle size and the lowest crystallinity have the lowest resistivity value in this study. Therefore, it is suggested that the electrical conductivity of the ATO films might be closely related to the ATO particle size and film density rather than crystallinity.

The sheet resistance and resistivity as a function of the solid content of the ATO sol is shown in Fig. 7. The resistivity decreased as the solid content increased to 8 wt% and then increased with higher solid content. The

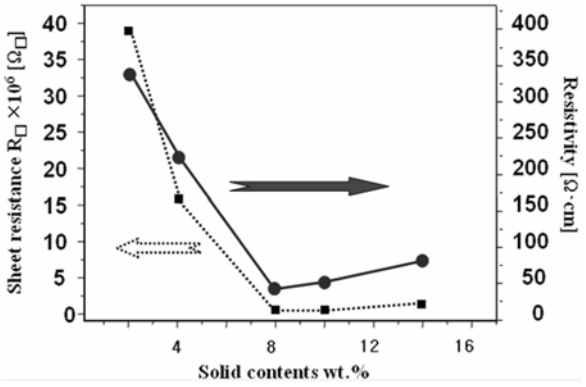

Fig. 7. Variations of sheet resistance and resistivity of ATO films with solid content of the ATO coating sol from 2 to 15 wt% at fixed antimony content of 10.0 mol%.

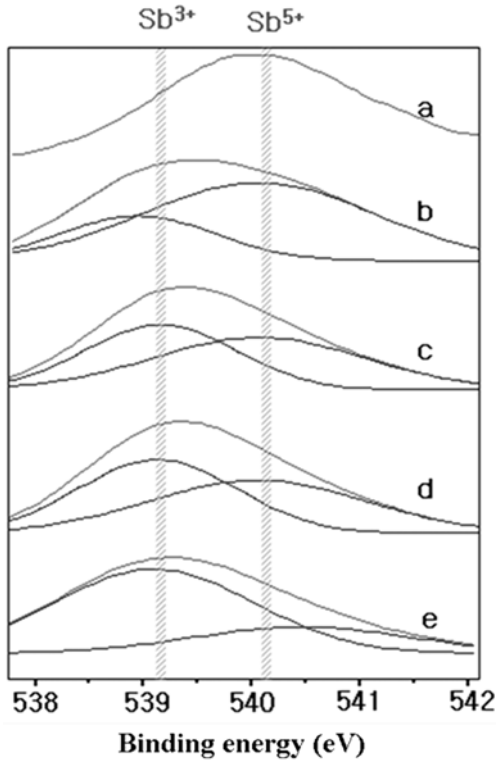

Fig. 8. XPS spectra of ATO films with various antimony contents; (a) 4, (b) 8, (c) 12, (d) 15, and (e) 20 mol% Sb.

resistivity initially decreased with increasing solid content because some amount of ATO particles was required to form a close-packed film of ATO particles by spin coating. Increasing the solid content above 8 wt% resulted in thicker films due to increased solution viscosity. This caused increased stress in the films as mentioned in the discussion of Fig. 4. Although visible cracks were only detected in the films with solid contents above 20 wt%, the increased thickness and stress in the films with solid contents above 8 wt% might cause defects in the close-packed structure of ATO particles such as microcracks. Therefore, we believe the electrical resistivity increased due to the induced stress when the sol with solid contents above the optimum value of 8 wt% was used.

Antimony can have various oxidation numbers such as Sb(III), Sb(IV), and Sb(V), where only Sb(V) can play an electron donor role like the n-type semiconductor in the Sn(IV) lattice. Therefore, the electrical resistivity of ATO films is also related to the oxidation number of Sb. If Sb(III) is also present in the Sb(V)-doped Sn(IV) lattice, Sb(III) will act as the electron acceptor and increase the resistivity. Therefore, XPS analysis was conducted to investigate the oxidation state of the Sb in the ATO films prepared in this study. As shown in Fig. 8, Sb(V) with its peak at 540.2 eV was dominant up to a Sb doping level of 8 mol%. The Sb(III) peak at 539.3 eV increased with additional Sb doping. Many researchers [39, 40] also attributed the increase of conductivity or electrical carrier concen-

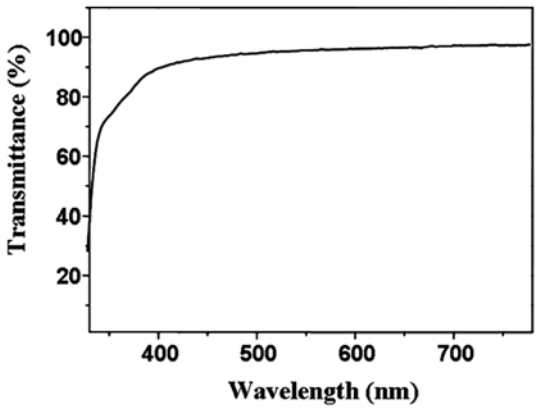

Fig. 9. UV-Vis transmittance spectra of the ATO film with 10 mol% of Sb-doped SnO_2 at a solid content of 8 wt%.

tration in ATO films to the lower amount of doped Sb(V) in the Sn(IV) lattice. They also observed an increased resistivity due to the increase of Sb(III) in the lattice at higher doping concentrations which agrees well with our results. Another hypothesis for increased resistivity above the optimum doping content of Sb is that excess antimony ions aggregate at the surface of the ATO particles as Sb(III) oxide or hydroxide causing the increased size of the ATO particles in the films. Therefore, the lowest resistivity value was obtained in the ATO film prepared from the sol with a Sb doping content of 10 mol% and solid content of 8 wt%.

The optical transmittance of the representative ATO films was analyzed by a UV/Vis spectrophotometer and the results are shown in Fig. 9. The transmittance of the ATO films was fairly high, above 90%, in the visible light range (400-800 nm). A rapid decrease of the transmittance below 400 nm was due to the absorption of light caused by the excitation of electrons from the valence band to the conduction band of SnO_2 which has a band gap energy of 3.60 eV [41]. In conclusion, transparent and conductive ATO films were successively prepared with the TMAH-stabilized ATO ethanol-based sol.

Summary

We have successfully synthesized ethanol-based ATO sols stable up to a solid content of 20 wt% by a peptization method with TMAH. The use of TMAH allowed the dried ATO nanoparticles to redisperse into the ethanol.

The electrical resistivity of the ATO films prepared by a spin coating method on PET was closely related to the size of the ATO particle, surface density of the film and the oxidation state of the antimony dopant. The lowest resistivity was obtained in the ATO film prepared from the sol with an antimony content and solid content of 10 mol% and 8 wt%, respectively.

We prepared transparent ATO films with a minimum resistivity value of 4.01×10^{1} Ω·cm using ethanol-based ATO sols with high stability and solid content without requiring a sintering process.

Acknowledgement

This work has been done with the support of the Korean Ministry of Commerce, Industry and Energy (project 10011473).

References

1. T.T. Emons, J.Q. Li, and L.F. Nazar, J. Am. Chem. Soc. 124 (2002) 8516-8517.
2. K.Y. Rajpure, M.N. Kusumade, M.N. Neumann Spallart, and C.H. Bhosale, Mater. Chem. Phys. 64 (2000) 184-188.
3. P.Y. Liu and H. Ye, J. Vac. Sci. Technol. 19 (2001) 1082-1085.
4. K. Osaza, T. Ye, and Y. Aoyagi, Thin Solid Films 246 (1994) 58-64.
5. S.S. Park, H. Zheng, and J.D. Mackenzie, Mater. Lett. 17 (1993) 346-352.
6. A. Nakajima, J. Mater. Sci. Lett. 12 (1993) 1778-1780.
7. M. Ippomatsu, H. Sasaki, and H. Yanagida, J. Mater. Sci. 25 (1990) 259-264.
8. S.S. Park and J.D. Mackenzie, Thin Solid Films 274 (1996) 154-159.
9. K.L. Copra and S.R. Das (Thin Solid Films Solar Cell, 1st Ed., 1983) p. 321.
10. D. Szczuko, J. Werner, S. Oswald, G. Behr, and K. Wetzig, Appl Surf. Sci. 179 (2001) 301-307.
11. B. Stjerna, E. Olsson, and C.G. Granqvist, J. Appl. Phys. 76 (1994) 3797-3817.
12. W.C. Las, N. Dolet, P. Dorpdor, and J.P. Bonnet, J. Appl. Phys. 74 (1993) 6191-6196.
13. C. Xu, J. Tamki, N. Miura, and N. Yamazoe, J. Mater. Sci. 27 (1992) 963-968.
14. S. Shanthi, C. Subramanian, and P. Ramasamy, J. Crystal Growth 194 (1998) 369-373.
15. J. Bruneax, H. Cachet, M. Forment, and M. Messad, Thin Solid Films 197 (1991) 129-142.
16. B. Orel, U. Laurencic-Stanger, Z. Crnjak-Orel, P. Bukovec, and M. Kosec, J. Non-Cryst. Solids 167 (1994) 272-288.
17. A.J. Freeman, K.R. Poeppelmeier, T.O. Mason, R.P.H. Chang, and T.J. Marks, MRS Bull. 25 (2000) 45-50.
18. M. Rami, E. Benamar, C. Messaoudi, D. Sayah, and A. Ennaoui, Eur. J. Solid State Inorg. Chem. 35 (1998) 211-215.
19. E.S. Mulla, H.S. Soni, V.J. Rao, and A.P.B. Sinha, J. Mater. Sci. 21 (1986) 1280-1287.
20. S.R. Reddy, A.K. Malik, and S.R. Jawalekar, Thin Solid Films 143 (1986) 113-118.
21. G. Sanon, ARajrup, and Mansingh, Thin Solid Films 190 (1990) 287-301.
22. B.S. Chiou, S.T. Hsieh, and W.F. Wu, J. Am. Ceram. Soc. 77 (1994) 1740-1742.
23. M. Mizuhashi, J. Non-Cryst. Solid 38-39 (1980) 329-334.
24. Z. Stryhal, J. Pavlik, S. Novak, A. Mackova, L. Perina, and K. Veltruska, Vacuum 67 (2002) 665-671.
25. J.C. Giuntini, W. Granier, J.V. Zanchetta, and A. Taha, J. Mater. Sci. Lett. 9 (1990) 1383-1388.
26. C. Terriera, J.P. Chatelona, R. Berjoanb, and J.A. Rogera, Thin Solid Films 263 (1995) 37-41.
27. A. Maddalena, R. Del Machio, S. Dir, and A. Raccanelli, J.

Non-Cryst. Solids 121 (1990) 365-369.
28. C. Su, T.K. Shew, Y.T. Cahng, M.A. Wan, M.C. Feng, and W.C. Hung, Synthetic Metals 153 (2005) 9-12.
29. M.A. Aegerter, A. Reich, D. Ganz, G. Gasparro, J. Piitz, and T. Krajewski, J. Non-Cryst. Solids 218 (1997) 123-128.
30. D. Vaufrey, M. Ben Khalifa, M.P. Besland, C. Sandu, M.D. Blanchin, V. Teodorescu, J.A. Roger, and J. Tardy, Synthetic Metals 127 (2002) 207-211.
31. M.J. Alam and D.C. Camerron, Thin Solid Films 377 (2000) 455-459.
32. M. Mattox, Thin Solid Films 204 (1991) 25-32.
33. C. Terriera, J.P. Chatelona, and J.A. Rogera, J. Sol-Gel Sci. and Technol. 10 (1997) 75-81.
34. Y. Takahashi and Y. Wada, J. Electrochem. Soc. 137 (1990) 267-271.
35. J. Puetz, F.N. Chalvet, G. Gasparro, N. Al-Dahoudi, and M.A. Aegerter, in "Emerging Field in Sol-Gel Science and Technology" (Kluwer Academic Publishers, 2003) p. 279.
36. D. Pyke, R. Reid, and R.J.D. Tiley, J. Solid State Chem. 25 (1978) 231-237.
37. G. Cao, in "Nanostructures & Nanomaterials-Synthesis, Properties & Applications" (Imperial College Press, 2004) p. 219.
38. S. Shanthi, C. Subramanian, and P. Ramasamy, J. Crystal Growth 197 (1999) 858-864.
39. D.J. Goyal, C. Agashe, B.R. Marathe, M.G. Takwal, and V.G. Bhide, J. Appl. Phys. 73 (1993) 520-525.
40. I.S. Mulla, H.S. Soni, V.J. Rao, and A.P.B. Sinha, J. Mater. Sci. 21 (1986) 280-284.
41. A. Svane and E. Antoncik, J. Phys. Chem. Solid 48 (1987) 171-175.